Hydrol. Earth Syst. Sci. Discuss., 12, 9977–10022, 2015
www.hydrol-earth-syst-sci-discuss.net/12/9977/2015/
doi:10.5194/hessd-12-9977-2015

Hydrology and Earth System Sciences
Open Access
Discussions

Investigating effects of different evapotranspiration (ET) schemes on soil water dynamics and ET partitioning: a large lysimeter case of summer maize in a semi-arid environment northwest of China

L. Yu[1,2], Y. Zeng[3], Z. Su[3], H. Cai[1,2], and Z. Zheng[1,2]

[1]Key Laboratory of Agricultural Soil and Water Engineering in Arid Area of Ministry of Education, Northwest Agriculture and Forestry University, Yangling, China
[2]Institute of Water Saving Agriculture in Arid Regions of China (IWSA), Northwest Agriculture and Forestry University, Yangling, China
[3]Faculty of Geo-Information Science and Earth Observation, University of Twente, Enschede, the Netherlands

Received: 10 August 2015 – Accepted: 3 September 2015 – Published: 29 September 2015

Correspondence to: H. Cai (caihj@nwsuaf.edu.cn)

Published by Copernicus Publications on behalf of the European Geosciences Union.

Abstract

Different evapotranspiration (ET) schemes can affect significantly the performance of land surface models in capturing the soil water dynamics and ET partitioning over various land cover and climates, the accurate understanding of which is crucial to determine the effective irrigation. In this study, a land model considering the coupled transfer of water, vapor and heat in the soil, with two alternative ET schemes, was used to investigate how the coupled mechanism can affect the soil water dynamics in a crop field and how the ET partitioning was influenced. There are two different evapotranspiration (ET) schemes, one is based on reference crop evapotranspiration (ET_0) and use LAI to partition into soil evaporation and transpiration, denoted as the ET_{ind} scheme; the other is one-step calculation of actual soil evaporation and potential transpiration by incorporating canopy minimum resistance and actual soil resistance into Penman–Monteith model, denoted as the ET_{dir} scheme. Results indicated that the coupled model with the two different ET schemes differed in simulating soil water content and crop evapotranspiration components while agreed well for the simulation of soil temperature. Considering the aerodynamic and surface resistance terms made the ET_{dir} scheme better in simulating soil evaporation especially after irrigations. Furthermore, the results of different crop growth scenarios indicated that the uncertainty in LAI played an important role in estimating the relative transpiration and evaporation fraction. The soil drying seemed to intensify the disturbance of maximum rooting depth and root growth rate in calculating ET components. The former was more important at the late growing season while the latter dominated at the early growing season.

1 Introduction

The soil water movement is the central physical process of the land surface models (LSMs), which interacts with surface infiltration, evaporation, root extraction and underground water recharge. Accurate description of this process is necessary for the appli-

HESSD
12, 9977–10022, 2015

cation of LSMs to achieve efficient and optimum water resources management. While it has been widely accepted that water vapor and heat transport should be coupled into the soil water model, especially in arid or semi-arid environment (Bittelli et al., 2008; Saito et al., 2006; Zeng et al., 2009a, b, 2011a, b), it is still not clear how such coupling can affect the soil water dynamics in crop fields, via different evapotranspiration (ET) schemes.

The ET plays a critical role in the process of soil water movement, as it controls the water distribution of surface and root zone soil layers through soil evaporation and transpiration. A common procedure to estimate ET is the so-called indirect ET scheme (ET_{ind}), which transfers the reference crop evapotranspiration (ET_0) into actual crop evapotranspiration (ET_c) using a simple multiplicative crop factor. Recent theoretical developments allow the adoption of a more robust Penman–Monteith (PM) equation description of ET. The direct ET scheme (ET_{dir}) is a one-step calculation procedure, which expresses the stomatal and aerodynamic controls in terms of various resistances in the PM equation. Independent from land surface models (LSMs), much effort has been made to compare the performances of different approaches to estimate ET (Federer et al., 1996; Stannard, 1993). The performance of different ET equations varied with the characteristics of land cover and climate (Shuttleworth and Wallace, 2009; Zhou et al., 2007). Ershadi et al. (2015) highlighted the need to provide guidance on selecting the appropriate ET method for use in a specific region.

Further evaluation confirmed that different ET schemes can significantly affect the performance of LSMs (Anothai et al., 2013; Chen et al., 2013; Federer et al., 1996; Kemp et al., 1997; Mastrocicco et al., 2010). Vörösmarty et al. (1998) made a comparison between reference surface (PETr) and surface cover-dependent (PETs) potential ET schemes in a global-scale water balance model (WBM) and concluded that WBM simulations were highly sensitive to the PET schemes and using the PETs methods would produce quite reasonable estimates of actual ET over a broad geographic domain. Recent assessment of HYDRUS-1-D model with different ET schemes indicated that using PM equation gave a better model performance in simulating soil water con-

HESSD
12, 9977–10022, 2015

tent (Mastrocicco et al., 2010). However, most of these results evaluated the model performances only for individual variable (e.g. soil water content or ET) or neglecting the heat or vapor transport effect (Anothai et al., 2013; Kemp et al., 1997; Vörösmarty et al., 1998).

The other fact is that the uncertainties of crop growth parameters were not fully tested although with a significant influence on the model performance (Federer et al., 2003). Previous studies generally concluded based on the combined analysis of the entire growing season (Padilla et al., 2011). However, these results could be inappropriate to some extent. Unlike the soil properties, the crop growth parameters had a significantly interactive effect with changing environment during the growing season (Teuling et al., 2006). The roughly seasonal assessment would conceal the crop modulating mechanism with changing environment.

The objectives in this paper are two fold: (i) investigating how different ET schemes will affect the soil water dynamics in a crop field located in Northwest China, semi-arid environment, with a coupled model considering transfer of water, vapor and heat in the soil, (ii) with the calibrated coupled model, the sensitivity analysis will be implemented to explore the influence of crop growth parameters on the ET portioning. In the following section, the field experiment, data collection and the numerical models will be introduced. The results were discussed in Sect. 3. The summary and conclusion were drawn in Sect. 4.

2 Material and method

2.1 Field experiment

The lysimeter experiment was conducted in the Yangling Irrigation Experiment Station located in northwest of China (34°17′ N, 108°04′ E, and elevation 521 m a.m.s.l. – above mean sea level). The experimental site is located at a semi-arid to sub-humid climatic region with a mean annual precipitation of 630 mm and a mean annual air temperature

HESSD
12, 9977–10022, 2015

of 12.9 °C. The soil at the location is silt clay loam with the field capacity of 23.5 % and the bulk density of 1.35 g cm^{-3}. The groundwater level is at least 50 m lower than the soil surface (Kang et al., 2001), thus the capillary rise from the groundwater can be neglected for the current study.

The lysimeter is made of steel with the size of 3 m length, 2.2 m width and 3 m depth. There are a filter layer, a weighing facility and a drainage system for measuring the amount of deep percolation at the bottom of the lysimeter. In order to apply the irrigation water, the steel wall is 5 cm higher than ground surface. The detailed description of the lysimeter is given in Fig. 1. A mobile rainproof shelter above the lysimeter was installed to control the precipitation. Summer maize was sown on 23 June and harvested on 2 October with the plant population of 40 plants within the area of 6.6 m^2. Irrigation was applied when soil water content dropped to a pre-set lower limit (i.e. 60 % of the field capacity). The amount of irrigation was crop ET measured by the lysimeter during the intervals of two irrigation events. Two supplemental irrigations were applied at the starting days (DOY 178 and 184) to ensure summer maize uniformly grow.

2.2 Data collection

Soil moisture and temperature was measured using the pre-calibrated sensors, which were installed at the depth of 20, 40, 60, 80, 100, 200, 225, 250 cm. Hourly measurements were made throughout the growing season. Considering the possible damage caused by tillage and other agricultural management, soil moisture and temperature sensors were not equipped at top soil layers. Top soil water content was measured using gravity oven method weekly. Crop ET was determined using the lysimeter weighting system (e.g. with the precision of 0.021 mm). The ET measurements were made hourly and summed to daily values during the growing season. Soil evaporation (E) was measured by weighing the micro-lysimeter at 08:00 LT daily. The micro-lysimeter was placed between two crop rows with the diameter of 12 cm and the depth of 20 cm. After significant precipitation and irrigation, we replaced the soil in the micro-lysimeter to keep the soil moisture in the micro-lysimeter similar to that of field conditions. Other

HESSD
12, 9977–10022, 2015

details are referred to previous studies over this lysimeter (Kang et al., 2003; Wang et al., 2007).

Meteorological data were obtained from a standard weather station located inside the experimental site. The data included daily maximum and minimum air temperature, air humidity, daily precipitation, sunny hours and wind speed at 10 m height. Hourly values of air temperature, air humidity and wind speed were generated from daily measurements using a trigonometric function, detail description can be found in Saito et al. (2006).

Leaf stomatal conductance was measured using the portable photosynthesis equipment (LI-6400, Li-Cor, USA) a few days after irrigation. Measurements were made on three functional leaves within the time intervals between 10:00–14:00 LT, when the stomatal conductance of summer maize reached its peak and kept steady (Zhang et al., 2011). Leaf area and plant height were measured from the average of at least 3 plant samples at intervals of 7–10 days starting at 14 days after planting. The crop stages or phenology were assessed following the recommendation by Allen et al. (1998). Dates for each crop development phase were shown in Table 1.

2.3 Numerical model

The STEMMUS (Simultaneous Transfer of Energy, Mass and Momentum in Unsaturated Soil) model was used to simulate coupled liquid water, water vapor and heat flow in unsaturated soil. In order to use STEMMUS for the lysimeter experiment, a macroscopic root water uptake module was incorporated into the STEMMUS.

2.3.1 STEMMUS

In STEMMUS, the extended version of Richards' equation with modification made by Milly (1982) was numerically solved to consider the vertical interactive process between atmosphere and soil. The governing equation of the liquid and vapor flow can be expressed as:

HESSD
12, 9977–10022, 2015

$$\frac{\partial}{\partial t}(\rho_L \theta_L + \rho_V \theta_V) = -\frac{\partial q_L}{\partial z} - \frac{\partial q_V}{\partial z} - S \quad (1)$$

where ρ_L and ρ_V ($kg\,m^{-3}$) are the density of liquid water and water vapor; θ_L and θ_V ($m^3\,m^{-3}$) are the volumetric water content (liquid and vapor); z (m) is the vertical space coordinate; q_L and q_V ($kg\,m^{-2}\,s^{-1}$) are the soil water fluxes of liquid and water vapor (positive upwards), respectively; and S (s^{-1}) is the sink term for the root water extraction.

The liquid water flux, separated into isothermal q_{Lh} (pressure head driven) and thermal q_{LT} (temperature driven), is described as:

$$q_L = q_{Lh} + q_{LT} = -K_{Lh}\left(\frac{\partial h}{\partial z} + 1\right) - K_{LT}\frac{\partial T}{\partial z} \quad (2)$$

where K_{Lh} ($m\,s^{-1}$) and K_{LT} ($m^2\,s^{-1}\,°C^{-1}$) are the isothermal and thermal hydraulic conductivities, respectively; h (m) is the pressure head; and T (°C) is the soil temperature. The water vapor flux, separated into isothermal q_{Vh} (pressure head driven) and thermal q_{VT} (temperature driven), is described as:

$$q_V = q_{Vh} + q_{VT} = -D_{Vh}\frac{\partial h}{\partial z} - D_{VT}\frac{\partial T}{\partial z} \quad (3)$$

where D_{Vh} ($kg\,m^{-2}\,s^{-1}$) is the isothermal vapor conductivity; and D_{VT} ($kg\,m^{-1}\,s^{-1}\,°C^{-1}$) is the thermal vapor diffusion coefficient, given in Zeng et al. (2011a).

The root water uptake term described by Feddes et al. (1978) is

$$S(h) = \alpha(h) S_p \quad (4)$$

where $\alpha(h)$ (dimensionless) is the reduction coefficient related to soil water potential; S_p (s^{-1}) is the potential water uptake rate.

$$S_p = b(x) T_p \quad (5)$$

HESSD
12, 9977–10022, 2015

where $b(x)$ is the normalized water uptake distribution, which describes the vertical variation of the potential extraction term, S_p, over the root zone, described in Šimůnek et al. (2008). T_p is the potential transpiration. Following De Vries (1958)'s work, the heat transport function in unsaturated soil can be expressed as

$$\frac{\partial}{\partial t}[(\rho_s\theta_s C_s + \rho_L\theta C_L + \rho_V\theta_V C_V)(T - T_r) + \rho_V\theta_V L_0] - \rho_L W\frac{\partial\theta}{\partial t} = \frac{\partial}{\partial z}\left(\lambda_{eff}\frac{\partial T}{\partial z}\right) - \frac{\partial q_L}{\partial z}C_L(T - T_r) - \frac{\partial q_V}{\partial z}[L_0 + C_V(T - T_r)] - C_L S(T - T_r) \quad (6)$$

where C_s, C_L and C_V ($J\,kg^{-1}\,°C^{-1}$) are the specific heat capacities of solids, liquid and water vapor, respectively; ρ_s ($kg\,m^{-3}$) is the density of solids; θ_s is the volumetric fraction of solids in the soil; T_r (°C) is the arbitrary reference temperature; L_0 ($J\,kg^{-1}$) is the latent heat of vaporization of water at temperature T_r; W ($J\,kg^{-1}$) is the differential heat of wetting (the amount of heat released when a small amount of free water is added to the soil matrix); and λ_{eff} ($W\,m^{-1}\,°C^{-1}$) is the effective thermal conductivity of the soil.

Dry air transport in unsaturated soil is originally taken into account in STEMMUS, the balance equation can be written as Thomas and Sansom (1995)

$$\frac{\partial}{\partial t}[\varepsilon\rho_{da}(S_a + H_c S_L)] = \frac{\partial}{\partial t}\left[D_e\frac{\partial\rho_{da}}{\partial z} + \rho_{da}\frac{S_a K_g}{\mu_a}\frac{\partial P_g}{\partial z} - H_c\rho_{da}\frac{q_L}{\rho_L} + (\theta_a D_{Vg})\frac{\partial\rho_{da}}{\partial z}\right] \quad (7)$$

where ε is the porosity; ρ_{da} ($kg\,m^{-3}$) is the density of dry air; S_a ($= 1 - S_L$) is the degree of air saturation in the soil; S_L ($= \theta_L/\varepsilon$) is the degree of saturation in the soil; H_c is the Henry's constant; D_e ($m^2\,s^{-1}$) is the molecular diffusivity of water vapor in soil; K_g (m^2) is the intrinsic air permeability; μ_a ($kg\,m^{-2}\,s^{-1}$) is the air viscosity; D_{Vg} ($m^2\,s^{-1}$) is the gas phase longitudinal dispersion coefficient. Note that the effects of dry air movement were not considered in the current study.

HESSD
12, 9977–10022, 2015

2.3.2 Initial and boundary conditions

In general, the soil surface water flow boundary can be characterized as a flux-type boundary controlling by the atmospheric forcing, including soil evaporation, precipitation and irrigation.

$$(q_L + q_V)|_{z=0} = E_s - \rho_L(P + I) \quad (8)$$

where E_s ($kg\,m^{-2}\,s^{-1}$) is the actual soil evaporation rate; P and I ($m\,s^{-1}$) are precipitation and irrigation rate, respectively.

After an intense irrigation or precipitation, ponding would occur at the soil surface, the surface boundary thus changed to a pressure-type boundary. It is assumed that surface runoff at the study site was negligible and the maximum height of the surface ponding layer was assigned 5 cm according to the lysimeter structure (Fig. 1). Since there is a filter layer at the bottom of the soil profile (Fig. 1), saturated water can be easily drained out of the lysimeter. The bottom boundary was considered as a seepage face condition (Šimůnek et al., 2008). The soil surface temperature deduced from the in-situ measurements was set as the upper boundary condition for the heat transfer, and the bottom temperature was fixed as the lower boundary condition. The initial soil moisture and temperature profile could be determined by interpolating the measured values at the starting day.

2.3.3 Transpiration and soil evaporation

Two different parameterizations of ET components were adopted in land surface models. A common procedure is based on reference crop evapotranspiration (ET_0) and then partition into soil evaporation and transpiration using crop factors (Feddes et al., 1974; Šimůnek et al., 2008; Wu et al., 1999), which was noted as the ET_{ind} scheme.

$$ET_0 = \frac{0.408(R_n - G) + \gamma \frac{900}{T_a+273} u_2(e_s - e_a)}{\Delta + \gamma(1 + 0.34u_2)} \quad (9)$$

HESSD
12, 9977–10022, 2015

where ET_0 (mm day^{-1}) is the reference ET; R_n (MJ m^{-2} day^{-1}) is the net radiation at the crop surface; G (MJ m^{-2} day^{-1}) is the soil heat flux density; T_a (°C) is the air temperature at 2 m height; u_2 (m s^{-1}) is the wind speed at 2 m height, can be obtained from wind speed data at 10 m height using a logarithmic wind profile function; e_a and e_s (kPa) are the actual and saturation vapour pressure; Δ (kPa °C^{-1}) is the slope of vapor pressure curve; γ (kPa °C^{-1}) is the psychrometric constant. The actual potential transpiration (T_p) can be estimated by multiplying ET_0 with the crop basal coefficient K_{cb}, describing the difference between actual and reference crop surface.

$$T_p = K_{cb} ET_0 \tag{10}$$

Several researches have related K_{cb} to the dynamics of vegetation (Er-Raki et al., 2007; González-Dugo and Mateos, 2008; Sánchez et al., 2012), the general expression defined by Duchemin et al. (2006) is

$$K_{cb} = K_{cb,\,max}(1 - \exp(-\tau LAI)) \tag{11}$$

where τ is the extinction coefficient, chosen as 0.6 (Kemp et al., 1997). Although τ may slightly change in responses to the structural differences in crop development (Allen et al., 1998; Tahiri et al., 2006), it is convenient here to consider τ as a constant (Allen et al., 1998; Shuttleworth and Wallace, 1985; Zhou et al., 2006). $K_{cb,\,max}$ is the basal crop coefficient at effective full ground cover.

Instead of the evaporation coefficient used in FAO dual $K_c - ET_0$, we adopted a simple evaporation parameterization similar to (Feddes et al., 1974; Kemp et al., 1997; Wu et al., 1999), in which the potential soil evaporation is given by Ritchie (1972)

$$E_p = \frac{\Delta}{\lambda(\Delta + \gamma)} R_n \exp(-0.39LAI) \tag{12}$$

where λ (MJ kg^{-1}) is the latent heat of vaporization. Actual soil evaporation can be achieved using a simple relationship proposed by Linacre (1973) and verified by Kemp

HESSD
12, 9977–10022, 2015

et al. (1997) for bare soil. Three successive stages are arbitrarily divided as:

$$
\begin{aligned}
E_s &= E_p && (\theta_1/\theta_{1,Fc}) > (E_p/k)^{1/2}, h_1 > -100\,000\,\text{cm} \\
E_s &= k(\theta_1/\theta_{1,Fc})^m && (\theta_1/\theta_{1,Fc}) \le (E_p/k)^{1/2}, h_1 > -100\,000\,\text{cm} \\
E_s &= k(\theta_{1+2}/\theta_{1+2,Fc})^m && h_1 \le -100\,000\,\text{cm}
\end{aligned} \tag{13}
$$

where θ_1 and $\theta_{1,Fc}$ are the actual volumetric water content and water content at field capacity of the top soil layer; h_1 (cm) is the water matric potential of top soil layer; k and m are the parameters primarily dependent on soil depth and soil texture, varying from 0.8 to 1 and 2 to 2.3, respectively, for a soil depth of 10 to 20 cm; θ_{1+2} and $\theta_{1+2,Fc}$ are the actual volumetric water content and water content at field capacity of the top 1st and 2nd soil layers.

The other scheme is one-step calculation of actual soil evaporation and potential transpiration by incorporating canopy minimum surface resistance and actual soil resistance into Penman–Monteith model. LAI is implicitly used to partition available energy into canopy and soil. We call it the ET_{dir} scheme. Compared to an alternative approach proposed by Shuttleworth and Wallace (1985), the interactive effect between canopy and soil was assumed negligible in the ET_{dir} scheme. This simplicity sounded reasonable, as indicated by Kemp et al. (1997) that no significant difference in simulating transpiration and soil evaporation was found for both schemes.

$$
T_p = \frac{\Delta\left(R_n^c - G\right) + \rho_a c_p \frac{(e_s - e_a)}{r_a^c}}{\lambda\left(\Delta + \gamma\left(1 + \frac{r_{cmin}}{r_a^c}\right)\right)} \tag{14}
$$

$$
E_s = \frac{\Delta\left(R_n^s - G\right) + \rho_a c_p \frac{(e_s - e_a)}{r_a^s}}{\lambda\left(\Delta + \gamma\left(1 + \frac{r_s}{r_a^s}\right)\right)} \tag{15}
$$

where R_n^c and R_n^s ($\text{MJ m}^{-2}\,\text{day}^{-1}$) are the net radiation at the canopy surface and soil surface, respectively; ρ_a (kg m^{-3}) is the air density; c_p ($\text{J kg}^{-1}\,\text{K}^{-1}$) is the specific

HESSD
12, 9977–10022, 2015

heat capacity of air; r_a^c and r_a^s ($s\,m^{-1}$) are the aerodynamic resistance for canopy surface and bared soil, respectively; r_{cmin} ($s\,m^{-1}$) is the minimum canopy surface resistance; r_s ($s\,m^{-1}$) is the soil surface resistance.

The net radiation reaching to the soil surface can be calculated using the Beer's law relationship of the form

$$R_n^s = R_n \exp(-\tau \mathrm{LAI}) \tag{16}$$

and the net radiation intercepted by the canopy surface is the residual part of total net radiation

$$R_n^c = R_n(1 - \exp(-\tau \mathrm{LAI})). \tag{17}$$

The minimum canopy surface resistance r_{cmin} is given by

$$r_{cmin} = r_{lmin}/\mathrm{LAI}_{eff} \tag{18}$$

where r_{lmin} is the minimum leaf stomatal resistance; LAI_{eff} is the effective leaf area index, which considers that generally the upper and sunlit leaves in the canopy actively contribute to the heat and vapor transfer. The soil surface resistance can be estimated using an exponential form proposed by Van De Griend and Owe (1994),

$$\begin{aligned} r_s &= r_{sl} && \theta_1 > \theta_{min}, h_1 > -100\,000\,\mathrm{cm}, \\ r_s &= r_{sl} e^{a(\theta_{min}-\theta_1)} && \theta_1 \le \theta_{min}, h_1 > -100\,000\,\mathrm{cm} \\ r_s &= \infty && h_1 \le -100\,000\,\mathrm{cm} \end{aligned} \tag{19}$$

where r_{sl} ($10\,s\,m^{-1}$) is the resistance to molecular diffusion of water surface; a (0.3565) is the fitted parameter; θ_1 is the topsoil water content; θ_{min} is minimum water content above which soil is able to deliver vapor at a potential rate.

HESSD
12, 9977–10022, 2015

2.4 Model parameters

2.4.1 Soil properties parameters

The Van Genuchten's analytical model (Van Genuchten, 1980) was used to simulate the soil moisture retention curve, which described the relationship between soil water potential and water content. Soil samples of top 20 cm were taken to obtain the parameters of the moisture retention curve.

Soil saturated hydraulic conductivity could be determined by laboratory method, which was 10.50 cm day^{-1}. This value is lower than the recommended value for silt clay loam (13.60 cm day^{-1}) by Saxton et al. (1986), but within the range of 10.30 to 14.30 cm day^{-1}, given by Wang et al. (2008) for the local soil. The soil hydraulic and thermal properties are given in Table 2.

2.4.2 Crop growth parameters

Leaf area index (LAI) was determined using measured leaf area. To simulate the seasonal dynamics of LAI, a linear interpretation was used between dates from the emergence to the first measurement and a simple quadratic function gave a good fitting for the measurements of LAI (R^2 = 0.96) (Fig. 2a). Effective leaf area index (LAI_{eff}), used in the ET_{dir} scheme, was equal to actual LAI when LAI was lower than 2 m^2 m^{-2}, and was assigned to half of the actual LAI for values higher than 4 and was assumed equal to 2 m^2 m^{-2} for the transition from 2 to 4 m^2 m^{-2} (Tahiri et al., 2006).

Maximum rooting depth was set to 1.2 m according to Allen et al. (1998). A classical logistic growth function was used to estimate root growth dynamics throughout the growing season, in which the root growth rate was determined from the assumption that 50 % of the rooting depth would be reached after 50 % of the growing season had elapsed, as described in Šimůnek et al. (2008) (see Fig. 2b for the root growth dynamics). The normalized water uptake distribution $b(x)$, which described the verti-

HESSD
12, 9977–10022, 2015

cal variation of the potential extraction term, S_p, over the root zone was determined following Šimůnek et al. (2008).

A piecewise linear function, defined in Feddes et al. (1978) and Feddes and Roats (2004), was used to describe the response of root to soil water potential $\alpha(h)$. The input water potential parameters were: (i) −15 cm for the water potential below which roots start to extract water, (ii) −30 cm for the water potential below which roots extract water at the maximum possible rate, (iii) higher limit −325 cm and lower limit −600 cm for the limiting water potential values below which roots can no longer extract water at the maximum rate (assuming a potential transpiration rate of 0.5 and 0.1 cm day^{-1}, respectively), (iv) −15 000 cm for the water potential below which root water uptake ceases.

2.5 Numerical simulations and experiments

The extended STEMMUS model was run using either the ET_{ind} scheme or the ET_{dir} scheme. Coupled water flow and heat transport equations were numerically solved using the Galerkin's finite element method for the spatial discretization and a fully implicit, backward difference approach for the temporal discretization. Plant root water uptake and soil water flow are fully coupled and equations are solved simultaneously at the same time step. The soil profile considered in this study was set to 3 m, as deep as the lysimeter, which was divided into 38 nodes with a finer discretization at upper soil layers (1 cm) than the lower soil layers (20 cm). Large lysimeter measurements, including soil moisture, soil temperature, ET and soil evaporation were used to assess the model performance. The validation of the soil water balance closure within the root zone gave an additional test of the effectiveness of the extended STEMMUS. In addition, since uncertainty may exist in the estimation of crop growth parameters, sensitivity test was implemented to explore how the simulation results vary with fluctuate precipitation and irrigation under different crop growth scenarios.

HESSD
12, 9977–10022, 2015

2.5.1 Water balance closure

The water balance closure was implemented by comparing soil water storage using two different methods. The direct method was based on the summation of soil water content over the root-zone

$$V_t = \sum_{\mathrm{rz}} \Delta x_i \frac{\theta_i + \theta_{i+1}}{2} \tag{20}$$

where V_t is the soil water storage in the root zone at the specific time t; Δx_i is the thickness of ith soil layer; θ_i and θ_{i+1} are model simulations of water content at the upper and lower surface of the ith soil layer, at the specific time t; $\sum_{\mathrm{rz}}$ represents the summation over the root zone.

Soil water storage could be also derived by the inversion of water balance equation within the root-zone

$$V_t = V_0 - \int_0^t T_{\mathrm{a}} \mathrm{d}t + \int_0^t (q_0 - q_N) \mathrm{d}t \tag{21}$$

where V_0 is the soil water storage in the root zone at initial time, calculated by the integration of initial soil moisture over the root zone; T_{a} is the actual crop transpiration, derived from the integration of root water uptake over the root zone; q_0 and q_N are simulated water flux at the surface and bottom of the root zone.

2.5.2 Crop growth scenarios

To investigate how biological factors control shallow soil water dynamics, three additional crop growth scenarios were used: (i) changed leaf area index (LAI), (ii) changed maximum rooting depth (Z_{rmax}) and (iii) changed root growth rate (R_{gr}) scenarios. The reference scenario (REF) was compared with changed LAI (LAI/LAI$_{_\mathrm{ref}}$), Z_{rmax} and R_{gr}

HESSD
12, 9977–10022, 2015

(Z_r/Z_{r_ref}) to show the impact of changed biological factors. These three growth parameters were set to a 20 % increase or decrease based on their reference values. The influence of a 20 % increase and decrease of LAI, Z_{rmax} and R_{gr} was shown in Fig. 2. The influence of 20 % increase of LAI on relative LAI_{eff} could be divided into three stages: (i) constantly 1.2 times larger stage, (ii) constantly equal stage, (iii) transition stage (Fig. 2b). The influence of 20 % decrease of LAI showed a similar three-stage trend. However, the 20 % decreased LAI (Fig. 2b, dash grey line) made the relative values of LAI_{eff} entered stage ii, i.e. constantly equal stage, later at the leaf growing stage while earlier at the leaf senescent stage than the 20 % increased LAI (Fig. 2b, solid grey line). Compared to the reference root depth dynamics, for the 20 % increased Z_{rmax} scenario, the relative values of root depth (Z_r/Z_{r_ref}) increased gradually until reached its maximum value at the late growing season. While for the 20 % increased R_{gr} scenario, the Z_r/Z_{r_ref} had a rapid increase up to the maximum value and then dropped down during the late growing season. On the contrary, the influence of a 20 % decrease of Z_{rmax} and R_{gr} showed opposite trends to the 20 % increase on the relative root depth dynamics. The influence of 20 % decreased R_{gr} showed a lag effect on the Z_r/Z_{r_ref} compared to the 20 % increase of R_{gr} (Fig. 2d). Thus, the values of Z_r/Z_{r_ref} for the 20 % decreased R_{gr} scenario were smaller at earlier growing season (before around DOY 196) while larger at late growing season (after around DOY 196) than the 20 % increased R_{gr} scenario.

2.6 Performance matrixes

To assess the model performance, several performance matrixes were used as in previous studies (Wei et al., 2015; Zhao et al., 2013). The determination coefficient R^2, achieved by performing a linear regression between observed and model simulated values; the root mean square error (RMSE), characterizing the variance of the model errors; as well as the index of agreement (d index) (Willmott, 1981; Willmott et al., 1985) could be computed as follows:

HESSD
12, 9977–10022, 2015

$$\mathrm{RMSE} = \sqrt{\frac{\sum_{i=1}^{n}(P_i - O_i)^2}{n}} \tag{22}$$

$$R^2 = \frac{\left[\sum_{i=1}^{n}\left(P_i - \overline{P}\right)\left(O_i - \overline{O}\right)\right]^2}{\sum_{i=1}^{n}\left(P_i - \overline{P}\right)^2 \sum_{i=1}^{n}\left(O_i - \overline{O}\right)^2} \tag{23}$$

$$d = 1 - \frac{\sum_{i=1}^{n}(P_i - O_i)^2}{\sum_{i=1}^{n}\left(\left|P_i - \overline{O}\right| + \left|O_i - \overline{O}\right|\right)^2} \tag{24}$$

where n is the number of observations, P_i and O_i are pairs of observed and model predicted values for a specific variable (soil water content, ET, etc.), $\overline{P}$ and $\overline{O}$ are the overall mean of observed and model predicted values. A good agreement between observed and model predicted values is characterized as a high value for the determination coefficient, d index and a low value for RMSE.

3 Results and discussion

3.1 Soil water content

Simulated soil water content, with two ET schemes, were compared with observations at the depth of 20, 40, 60, 80 and 100 cm (Fig. 3). The soil water content at the 20 cm with the $\mathrm{ET}_{\mathrm{ind}}$ scheme was in good agreement with the observation. Though a slight underestimation at the initial stage, the effects of incoming water flux (precipitation and

HESSD
12, 9977–10022, 2015

irrigation) on soil water dynamics were well represented, as evidenced with d index of 0.81 and RMSE of 0.017 $cm^3\,cm^{-3}$. For the deeper soil layers, however, sensor-observed fluctuations of soil water content were much smaller when compared to simulated values, thus induced large discrepancies. The values for d index ranged from 0.26 to 0.66 and RMSE ranged from 0.019 to 0.025 $cm^3\,cm^{-3}$ for the soil depth from 40 to 100 cm.

Soil water content simulated with the ET_{dir} scheme had similar results as with the ET_{ind} scheme (Fig. 3). However, owning to more underestimation, the model with ET_{dir} scheme performed a little worse than with the ET_{ind} scheme. The d index values ranged from 0.20 to 0.73 and RMSE ranged from 0.020 to 0.036 $cm^3\ cm^{-3}$ for the soil depth from 20 to 100 cm.

Using both ET schemes, the extended STEMMUS model underestimated soil water content at early the growing season. From the point of water balance, this underestimation may be explained by more soil water consumption mainly due to topsoil evaporation, indicating that both ET schemes overestimated soil evaporation at early the growing season. The other possible reason was that the irrigation applied during this period was too small to be uniformly distributed and thus single-point soil moisture observation lost its ability to represent the heterogeneous soil moisture variations. Such underestimation disappeared when large amount of water was applied at later the growing season (Fig. 3, 20 cm).

The discrepancies increased with soil depth for both ET schemes. The reason lay here may be two-fold. On one hand, the soil moisture observations were doubtable, as no significant fluctuation with irrigation occurred at deeper soil layers, which was also inconsistent with the results for the same experiment site (Kang et al., 2001). The doubtable observations may be linked to the installing position of the soil moisture sensors (either equipped at positions dominated by preferential flow or adjacent to the macropores). On the other hand, the assumption of homogeneous soil texture was inappropriate as discussed by previous studies (Zeng et al., 2011a). Soil hydraulic

HESSD
12, 9977–10022, 2015

parameters controlled the liquid water flux partition through soil layers, larger infiltration rate could result in greater fluctuation of soil water content at deeper soil layers.

3.2 Root zone water balance

According to Eqs. (20) and (21), simulated soil water storage based on the integration of soil water content and the inversion of water balance equation over the root-zone with two ET scheme were compared in Fig. 4. Soil water storage calculated with both schemes agreed well for the ET_{ind} scheme. The value of RMSE was 5.88 mm and the *d* index value was 0.98. Similarly, a good agreement was found when using the ET_{dir} scheme with values of RMSE and *d* index equaled to 5.13 mm and 0.99. Overall, the results based on the performance matrixes and the visual comparison of soil water storage dynamics revealed that the numerical solution using both the ET_{ind} and ET_{dir} scheme effectively reproduced the closure of water balance even under dramatically changed surface boundary flux conditions.

Simulated results using two ET schemes showed similar trends of soil water storage throughout the growing season (Fig. 4). As expected, the largest increases occurred after large irrigations. Using the ET_{dir} scheme tended to result in lower soil water storage than the ET_{ind} scheme. The differences between two ET schemes were generally increasing while soil drying.

3.3 Soil temperature

Figure 5 presented the dynamics of sensor-observed and the simulated soil temperature with two ET schemes at various soil depths. Compared to the observation, the simulation with both ET schemes started with a good agreement and followed with a slight overestimation after the first main irrigation. Irrigation events had a significant impact on the soil temperature simulation due to the uncertainties of soil surface temperature. Nevertheless, the seasonal variations of soil temperature could be satisfactorily achieved with both ET schemes. The overall *d* index values, for the soil depth from

HESSD
12, 9977–10022, 2015

20 to 100 cm, ranged from 0.76 to 0.95 with the ET_{ind} scheme and 0.78 to 0.95 with the ET_{dir} scheme. The values of RMSE ranged from 1.19 to 1.71 °C with the ET_{ind} scheme and 1.14 to 1.61 °C with the ET_{dir} scheme for the soil depth from 20 to 100 cm.

3.4 Estimation of ET

Combined with simulation results of soil water content, accurate ET estimates could help with the visualization of soil water balance, reduce deep percolation, improve irrigation efficiency and ultimately optimize water resources management. Therefore, the capability of the extended STEMMUS model with different ET schemes in reproducing the dynamics of ET is of great importance and requires fully evaluation with observed ET data.

3.4.1 ET at hourly time scale

The performance of both ET schemes to estimate the diurnal pattern of ET throughout the growing season was shown in Fig. 6a–c and Table 3. The hourly ET rates simulated using the ET_{ind} scheme generally agreed well with lysimeter-observed ones (Fig. 6a). The comparison at hourly time scale in Fig. 6a indicated that the ET_{ind} scheme tended to underestimate ET after main irrigation events. The largest underestimation was found after the third main irrigation, occurring at the mid-season of the maize growth stage. The results summarized in Table 3 suggested that the greatest disagreement among the growth stages was found at the initial stage with the values of *d* index and RMSE being 0.84 and 0.10 $mm\,h^{-1}$, compared to 0.94 and 0.11 $mm\,h^{-1}$, 0.93 and 0.11 $mm\,h^{-1}$, 0.90 and 0.07 $mm\,h^{-1}$ during other development stages.

Compared to the ET_{ind} scheme, the ET_{dir} scheme performed better in simulating hourly revolution of ET over the entire maize growing season (Fig. 6b and Table 3). There was no significant underestimation after main irrigation events. The main disagreement for the ET_{dir} scheme occurred at early the growing stage. The values for *d* index and RMSE were 0.90 and 0.10 $mm\,h^{-1}$, 0.96 and 0.09 $mm\,h^{-1}$, 0.98 and

HESSD
12, 9977–10022, 2015

0.08 mm h^{-1}, 0.93 and 0.06 mm h^{-1} for the initial, crop development, mid-season and late season growing stages, respectively.

Furthermore, Fig. 6c presented a detail diurnal pattern of observed and simulated ET at mid-season stage, in which two ET schemes showed different behaviors after irrigation. Better performance was achieved using the ET_{dir} scheme when compared to the ET_{ind} scheme. For the ET_{ind} scheme, significant underestimation was found at mid-day hours when the ET rates greater than 0.5 mm h^{-1}. This underestimation could be explained by the underestimated soil evaporation during this period (see Fig. 8), indicating that the parameterization of soil evaporation in the ET_{ind} scheme was inappropriate during high water demand conditions. Considering the aerodynamic component, the ET_{dir} scheme showed a reasonable representation of hourly ET rates. Nevertheless, the main diurnal patterns simulated using the ET_{ind} scheme agreed with observed ET variations as well as the ET_{dir} scheme except for the high water consumption periods.

3.4.2 ET at daily time scale

Compared to lysimeter observed daily ET rates, both ET schemes showed similar trends over the entire growing season (Fig. 7). Lacking of considering the blocking effects of stochastic clouds on the net radiation, large overestimation of ET rates for both schemes would occur on some cloudy days (Fig. 6, DOY 196, 197, 221 and 241). Daily ET rates simulated with the ET_{dir} scheme had a more fluctuation than the ET_{ind} scheme. Moreover, two ET schemes differed in the crop stage-specific behavior. There was an average underestimation for the ET_{ind} scheme while a slight overestimation for the ET_{dir} scheme at initial growing season. Daily ET rates at mid-season growth season tended to be underestimated by the ET_{ind} scheme while successfully described by the ET_{dir} scheme. Overall, daily ET rates simulated by the ET_{dir} scheme performed better than the ET_{ind} scheme as indicated by the *d* index and RMSE values being 0.96 and 0.74 mm day^{-1} for the ET_{dir} scheme, while 0.89 and 1.06 mm day^{-1} for the ET_{ind} scheme.

HESSD
12, 9977–10022, 2015

Observed soil evaporation with micro-lysimeter was used to assess the performance of both ET schemes to simulate soil evaporation (Fig. 8). Statistical results indicated the ET_{dir} scheme had a closer agreement than the ET_{ind} scheme with values of RMSE and d index being 0.51 mm day^{-1} and 0.84, 0.73 mm day^{-1} and 0.64. Unfortunately, during periods between two supplemental irrigations at early the growing season (DOY 177–183), the soil evaporation measured by the micro-lysimeter was not available. Thus, it was difficult to make a conclusion on the model performance during this period. At late the growing season, using both ET schemes tended to underestimate daily evaporation rates after main irrigation events. Such underestimation may be caused by the use of micro-lysimeter. The observed soil evaporation may be higher than the actual soil evaporation, since the micro-lysimeter cut off the soil water loss due to the root water extraction in the evaporative soil layer. The similar behavior was reported for maize by Zhao et al. (2013) and Wei et al. (2015) at the same latitude sites. Compared to the ET_{dir} scheme, using the ET_{ind} scheme resulted in a much lower values of evaporation rates, especially after irrigations at the initial and mid-late growing season (see also Table 4). During these periods, the local irrigations intensified the vertial vapor gradient and the relative sparse vegetation cover highlighted the importance of aerodynamics component. Thus, larger underestimation and less fluctuation of soil evaporation with the ET_{ind} scheme could be partially explained by the simplification of aerodynamic and surface resistance components in the calculation.

3.4.3 Cumulative ET

A comparison between cumulative ET of observed and simulated using the ET_{ind} and ET_{dir} scheme was shown in Fig. 9. The cumulative ET for lysimeter observed, ET_{ind} and ET_{dir} simulated are 334.18, 369.37 and 354.89 mm, respectively. Both ET schemes overestimated seasonal ET when compared to lysimeter observations. Two periods, crop development and late season stage, were contributed to the overestimation when using the ET_{ind} scheme. While for the ET_{dir} scheme the primary overestimation appeared at initial and crop development stage, accounting for 70 % of the overestima-

HESSD
12, 9977–10022, 2015

tion (Table 4). The deviation of total ET to the observed value for the ET_{dir} scheme was greater than the ET_{ind} scheme, 35.18 and 20.71 mm, respectively. This nearly 15 mm difference was mainly attributed to a larger amount of evaporation for the ET_{dir} scheme during the initial growth stage (Table 4), which consequently resulted in more severe soil water depletion (Fig. 3, 20 cm).

3.4.4 Characteristics of ET partitioning

Crop stage-specific soil evaporation (E), plant transpiration (T), evapotranspiration (ET) and evaporation fraction (E/ET, EF) were presented in Table 4. Similar to previous studies (Kang et al., 2003; Zhao et al., 2013), the proportion of evaporation (e.g. the evaporation fraction) was largest at the initial stage, then decreased over crop development and reached its smallest value at mid-season stage, whereas a significant rebound was found during the late season. The dynamic role of evaporation was mainly attributed to the crop vegetation development (Hu et al., 2009; Liu et al., 2002). The evaporation fraction of four development stages ranged from 24.38 to 86.58 % for the ET_{dir} scheme and 10.31 to 81.01 % for the ET_{ind} scheme, similar to previously published results (Paredes et al., 2015; Wei et al., 2015; Zhao et al., 2013). Some differences were found in simulating individual components of crop ET when using two different ET schemes. The ET_{dir} scheme showed a larger evaporation and smaller transpiration than the ET_{ind} scheme throughout the growing season, resulting in an overall greater evaporation fraction.

The overall evaporation fraction for both ET schemes was 24.05 and 36.44 %, lower than the range from 43.57 to 52.52 %, a 4 year field observations in the same region but with significantly higher frequency of wetting events (Wang et al., 2007), close to observations of 30.3 % (Liu et al., 2002) and 33 % (Kang et al., 2003) and within the range of 20 to 40 %, reviewed by Kool et al. (2014) for most of row crops.

HESSD
12, 9977–10022, 2015

3.5 Crop growth scenarios

To investigate the uncertainty of crop growth parameters, different crop growth scenarios introduced in Sect. 2.5.2 were adopted to run the STEMMUS with both ET schemes (Fig. 10). The reference scenario (REF) was compared to changed LAI, Z_{rmax} and R_{gr} scenarios. The relative values (e.g. T/T_{ref} and EF/EF_{ref}) were used here to facilitate comparisons between parameters and scenarios.

Under the changed LAI scenario, the dynamics of seasonal relative values of transpiration (T/T_{ref}) was a tradeoff between increasing LAI and decreasing soil water availability while other factors maintained unchanged throughout the growing season. It was showed in Fig. 10a that, for the ET_{ind} scheme, the sensitivity of transpiration to LAI decreased until its value approached to $2\,m^2\,m^{-2}$, leveled off as both factors were equally important and finally elevated as soil water availability was decreasing. For the ET_{ind} scheme, more sensitive to LAI was presented at early the growing season, which was consistent with previous studies. In Fig. 10 g, the dynamics of the relative values of evaporation fraction (EF/EF_{ref}) showed a similar trend with the seasonal variation of LAI (Fig. 2a), indicating that small differences in soil water availability appeared to have a negligible effect on the relative evaporation fraction (EF/EF_{ref}) over the entire growing season. The LAI dynamics could explain much of the seasonal variation of the relative EF. It was worth to be noted that there was an asymmetry variation of relative EF for the same LAI disturbance, indicating that EF was nonlinearly dependent on LAI disturbance (Fig. 10g).

For the ET_{dir} scheme, more complicated behavior of the relative transpiration than the ET_{ind} scheme was showed (Fig. 10d). Compared to the ET_{ind} scheme, similar trend of the sensitivity of relative transpiration to LAI was found when LAI dominated at the early growing season. More fluctuation was showed at the middle season. A suppression effect appeared at the end of growing season (i.e. Increasing LAI resulted in lower transpiration than the reference scenario). This behavior could be explained by the different selection of LAI in estimating transpiration between two ET schemes (LAI

HESSD
12, 9977–10022, 2015

for ET_{ind} scheme, LAI_{eff} for ET_{dir} scheme) (Fig. 2a). Compared to the ET_{ind} scheme, the response of relative EF to LAI showed similar trends at early the growing season with a less sensitivity for the ET_{dir} scheme. Differences were found at late the growing season with a negligible effect of LAI on relative EF when the maize got senescent (Fig. 10j).

Under the changed maximum rooting depth and root growth rate scenarios, the interactive effects of root depth dynamics and soil water availability on transpiration and evaporation fraction were explored. Seasonal transpiration ratio was an increasing function of soil water depletion until reaching its threshold in both scenarios. The effects of changed maximum rooting depth on relative transpiration and evaporation fraction were elevated as the soil was drying. Larger sensitivity was found at late the growing stage. On the contrary, the influence of soil drying on the sensitivity of transpiration and evaporation fraction to root growth rate was decreasing until no significant effects was found when the root reached its maximum depth. The most influenced period occurred at the early growing season. This behavior can be explained by the difference of root depth dynamics in both scenarios. As shown in Fig. 2b and c, the effects of changing maximum rooting depth is increasing until reach its maximum value at late the growing season while the effects of changing root growth rate primarily dominates at the early growing season. Furthermore, there was an asymmetric variation of relative transpiration and evaporation fraction for the same disturbance of root growth rate, larger variation for conditions of decreasing root growth rate by 20 % while less variation for the increasing conditions (especially at DOY 225, in Fig. 10c, f, i, and l). Such asymmetric variation can be explained by the lag effect described in Sect. 2.5.2. Two ET schemes differed in their variations of sensitivity to root growth parameters, with a higher sensitivity for the ET_{dir} scheme with the same parameter disturbance. This is probably due to the ET_{dir} scheme is more sensitive to soil water depletion than the ET_{ind} scheme (Fig. 3), with the consideration of aerodynamic and surface resistances.

Based on the crop growth scenarios results, some suggestions could be presented to reduce the proportion of soil evaporation in total evapotranspiration. Under the same

HESSD
12, 9977–10022, 2015

irrigation and atmospheric forcing conditions, we can increase the leaf area index by properly increasing the planting density (Fig. 10g and j). Unlike the LAI, the sensitivity of transpiration to root growth parameters depended more on the soil water depletion, which indicated that the effects of dynamic root growth parameters should not be dismissed in arid environment. In fact, a variety of maximum rooting depth values were reported for maize previously (Canadell et al., 1996; Hsiao et al., 2009; Liu et al., 1998), due to different genotypes and rhizosphere environment. Under conditions of soil drying, plants tend to increase root depth to maintain a certain of water extraction (Hund et al., 2009; Verma et al., 2014), which was also evidenced with Fig. 10b, c, e and f.

4 Summary and conclusion

With the in situ data collected in a large lysimeter experiment, we used the extended STEMMUS model in a semi-arid environment to investigate how the coupling transfer of water, vapor and heat in the soil can affect the soil water dynamics in a crop field, with different evapotranspiration schemes (ET_{ind} and ET_{dir}). The simulated soil water content using the ET_{ind} scheme had a closer agreement than those simulated with the ET_{dir} scheme when compared with measured values at the 20 cm soil depth. However, disagreements increased for deeper soil layers, either the inaccuracy of soil moisture observations or the heterogeneity of soil hydraulic parameters was responsible for the discrepancies and required further investigation. Simulation of soil temperature was relatively good for both ET schemes.

Evaluating the performance of the two ET schemes in estimating hourly, daily and cumulative evapotranspiration showed that the ET_{dir} scheme performed better except for the cumulative evapotranspiration, 15 mm more overestimation, than the ET_{ind} scheme when compared to lysimeter observations. Caution should be taken in partitioning ET, because individual ET components (soil evaporation, transpiration) were not fully or accurately measured. This study suggests that the ET_{dir} scheme gave better simulation of soil evaporation than the ET_{ind} scheme, especially at the late growing season.

HESSD
12, 9977–10022, 2015

It confirmed that the aerodynamic and surface resistance terms were necessary for evaporation estimation.

The crop growth scenarios results revealed the interactive effects of LAI, maximum rooting depth and root growth rate with soil water availability on relative transpiration and evaporation fraction. When LAI is smaller than $2\,m^2\,m^{-2}$, LAI played an important role in controlling transpiration. The effects of maximum rooting depth and root growth rate only functioned at drying period, the former was more important at late the growing season while the latter dominated at the early growing season. As the disturbance of crop growth parameters has a significant effect on the simulation results, further consideration of the dynamics of crop growth parameters with changing environment is needed.

Acknowledgements. This research was supported by the National Natural Science Foundation of China (Grant No. 51179162) and the 111 Project of Chinese Education Ministry (No. B12007). We thank the anonymous referees very much for improving the manuscript. L. Yu is grateful for the financial support by the China Scholarship Council (CSC), No. 201406300115.

References

Allen, R. G., Pereira, L. S., Raes, D., and Smith, M.: Crop evapotranspiration – Guidelines for computing crop water requirements – FAO Irrigation and drainage paper 56, FAO, Rome, 300 pp., 1998.

Anothai, J., Soler, C. M. T., Green, A., Trout, T. J., and Hoogenboom, G.: Evaluation of two evapotranspiration approaches simulated with the CSM-CERES-Maize model under different irrigation strategies and the impact on maize growth, development and soil moisture content for semi-arid conditions, Agr. Forest Meteorol., 176, 64–76, 2013.

Bittelli, M., Ventura, F., Campbell, G. S., Snyder, R. L., Gallegati, F., and Pisa, P. R.: Coupling of heat, water vapor, and liquid water fluxes to compute evaporation in bare soils, J. Hydrol., 362, 191–205, 2008.

HESSD

12, 9977–10022, 2015

Canadell, J., Jackson, R. B., Ehleringer, J. B., Mooney, H. A., Sala, O. E., and Schulze, E. D.: Maximum rooting depth of vegetation types at the global scale, Oecologia, 108, 583–595, 1996.

Chen, J., Chen, B., Black, T. A., Innes, J. L., Wang, G., Kiely, G., Hirano, T., and Wohlfahrt, G.: Comparison of terrestrial evapotranspiration estimates using the mass transfer and Penman–Monteith equations in land surface models, J. Geophys. Res.-Biogeo., 118, 1715–1731, 2013.

De Vries, D. A.: Simultaneous transfer of heat and moisture in porous media, EOS T. Am. Geophys. Un., 39, 909–916, 1958.

De Vries, D. A.: Thermal properties of soils, in: Physics of Plant Environment, edited by: van Wijk, W. R., North-Holland Publishing Company, Amsterdam, 1963.

Duchemin, B., Hadria, R., Erraki, S., Boulet, G., Maisongrande, P., Chehbouni, A., Escadafal, R., Ezzahar, J., Hoedjes, J. C. B., Kharrou, M. H., Khabba, S., Mougenot, B., Olioso, A., Rodriguez, J. C., and Simonneaux, V.: Monitoring wheat phenology and irrigation in Central Morocco: on the use of relationships between evapotranspiration, crops coefficients, leaf area index and remotely-sensed vegetation indices, Agr. Water Manage., 79, 1–27, 2006.

Er-Raki, S., Chehbouni, A., Guemouria, N., Duchemin, B., Ezzahar, J., and Hadria, R.: Combining FAO-56 model and ground-based remote sensing to estimate water consumptions of wheat crops in a semi-arid region, Agr. Water Manage., 87, 41–54, 2007.

Ershadi, A., McCabe, M. F., Evans, J. P., and Wood, E. F.: Impact of model structure and parameterization on Penman–Monteith type evaporation models, J. Hydrol., 525, 521–535, 2015.

Feddes, R. A. and Roats, P. A. C.: Parameterizing the soil-water-plant root system, in: Unsaturated-Zone Modeling: Progress, Challenges and Applications, edited by: Feddes, R. A., DeRooij, G. H., and VanDam, J. C., Kluwer Academic Publishers, Dordrecht, the Netherlands, 95–141, 2004.

Feddes, R. A., Bresler, E., and Neuman, S. P.: Field test of a modified numerical model for water uptake by root systems, Water Resour. Res., 10, 1199–1206, 1974.

Feddes, R. A., Kowalik, P. J., and Zaradny, H.: Simulation of Field Water Use and Crop Yield, Centre for Agricultural Publishing and Documentation, Wageningen, the Netherlands, 1978.

HESSD
12, 9977–10022, 2015

Federer, C. A., Vörösmarty, C., and Fekete, B.: Intercomparison of methods for calculating potential evaporation in regional and global water balance models, Water Resour. Res., 32, 2315–2321, 1996.
Federer, C. A., Vörösmarty, C., and Fekete, B.: Sensitivity of annual evaporation to soil and root properties in two models of contrasting complexity, J. Hydrometeorol., 4, 1276–1290, 2003.
González-Dugo, M. P. and Mateos, L.: Spectral vegetation indices for benchmarking water productivity of irrigated cotton and sugarbeet crops, Agr. Water Manage., 95, 48–58, 2008.
Hsiao, T. C., Heng, L., Steduto, P., Rojas-Lara, B., Raes, D., and Fereres, E.: AquaCrop – the FAO crop model to simulate yield response to water: III. Parameterization and testing for maize, Agron. J., 101, 448–459, 2009.
Hu, Z., Yu, G., Zhou, Y., Sun, X., Li, Y., Shi, P., Wang, Y., Song, X., Zheng, Z., Zhang, L., and Li, S.: Partitioning of evapotranspiration and its controls in four grassland ecosystems: application of a two-source model, Agr. Forest Meteorol., 149, 1410–1420, 2009.
Hund, A., Ruta, N., and Liedgens, M.: Rooting depth and water use efficiency of tropical maize inbred lines, differing in drought tolerance, Plant Soil, 318, 311–325, 2009.
Kang, S., Zhang, F., and Zhang, J.: A simulation model of water dynamics in winter wheat field and its application in a semiarid region, Agr. Water Manage., 49, 115–129, 2001.
Kang, S., Gu, B., Du, T., and Zhang, J.: Crop coefficient and ratio of transpiration to evapotranspiration of winter wheat and maize in a semi-humid region, Agr. Water Manage., 59, 239–254, 2003.
Kemp, P. R., Reynolds, J. F., Pachepsky, Y., and Chen, J. L.: A comparative modeling study of soil water dynamics in a desert ecosystem, Water Resour. Res., 33, 73–90, 1997.
Kool, D., Agam, N., Lazarovitch, N., Heitman, J. L., Sauer, T. J., and Ben-Gal, A.: A review of approaches for evapotranspiration partitioning, Agr. Forest Meteorol., 184, 56–70, 2014.
Linacre, E. T.: A simpler empirical expression for actual evapotranspiration rates – a discussion, Agr. Meteorol., 11, 451–452, 1973.
Liu, C., Zhang, X., and Zhang, Y.: Determination of daily evaporation and evapotranspiration of winter wheat and maize by large-scale weighing lysimeter and micro-lysimeter, Agr. Forest Meteorol., 111, 109–120, 2002.
Liu, Y., Teixeira, J. L., Zhang, H. J., and Pereira, L. S.: Model validation and crop coefficients for irrigation scheduling in the North China plain, Agr. Water Manage., 36, 233–246, 1998.

HESSD
12, 9977–10022, 2015

Mastrocicco, M., Colombani, N., Salemi, E., and Castaldelli, G.: Numerical assessment of effective evapotranspiration from maize plots to estimate groundwater recharge in lowlands, Agr. Water Manage., 97, 1389–1398, 2010.
Milly, P. C. D.: Moisture and heat transport in hysteretic, inhomogeneous porous media: a matric head-based formulation and a numerical model, Water Resour. Res., 18, 489–498, 1982.
Padilla, F. L. M., González-Dugo, M. P., Gavilán, P., and Domínguez, J.: Integration of vegetation indices into a water balance model to estimate evapotranspiration of wheat and corn, Hydrol. Earth Syst. Sci., 15, 1213–1225, doi:10.5194/hess-15-1213-2011, 2011.
Paredes, P., Wei, Z., Liu, Y., Xu, D., Xin, Y., Zhang, B., and Pereira, L. S.: Performance assessment of the FAO aquaCrop model for soil water, soil evaporation, biomass and yield of soybeans in north china plain, Agr. Water Manage., 152, 57–71, 2015.
Ritchie, J. T.: Model for predicting evaporation from a row crop with incomplete cover, Water Resour. Res., 8, 1204–1213, 1972.
Saito, H., Šimůnek, J., and Mohanty, B. P.: Numerical analysis of coupled water, vapor, and heat transport in the vadose zone, Vadose Zone J., 5, 784–800, 2006.
Sánchez, N., Martínez-Fernández, J., González-Piqueras, J., González-Dugo, M. P., Baroncini-Turrichia, G., Torres, E., Calera, A., and Pérez-Gutiérrez, C.: Water balance at plot scale for soil moisture estimation using vegetation parameters, Agr. Forest Meteorol., 166–167, 1–9, 2012.
Saxton, K. E., Rawls, W. J., Romberger, J. S., and Papendick, R. I.: Estimating generalized soil-water characteristics from texture, Soil Sci. Soc. Am. J., 50, 1031–1036, 1986.
Shuttleworth, W. J. and Wallace, J. S.: Evaporation from sparse crops – an energy combination theory, Q. J. Roy. Meteorol. Soc., 111, 839–855, 1985.
Shuttleworth, W. J. and Wallace, J. S.: Calculating the water requirements of irrigated crops in Australia using the matt-shuttleworth approach, T. ASABE, 52, 1895–1906, 2009.
Šimůnek, J., Šejna, M., Saito, H., Sakai, M., and van Genuchten, M. T.: The HYDRUS-1-D software package for simulating the movement of water, heat, and multiple solutes in variably saturated media, version 4.0, HYDRUS software series 3, Department of Environmental Sciences, University of California Riverside, Riverside, California, USA, 315 pp., 2008.
Stannard, D. I.: Comparison of Penman–Monteith, Shuttleworth–Wallace, and modified Priestley–Taylor evapotranspiration models for wildland vegetation in semiarid rangeland, Water Resour. Res., 29, 1379–1392, 1993.

HESSD
12, 9977–10022, 2015

Tahiri, A. Z., Anyoji, H., and Yasuda, H.: Fixed and variable light extinction coefficients for estimating plant transpiration and soil evaporation under irrigated maize, Agr. Water Manage., 84, 186–192, 2006.
Teuling, A. J., Uijlenhoet, R., Hupert, F., and Troch, P. A.: Impact of plant water uptake strategy on soil moisture and evapotranspiration dynamics during drydown, Geophys. Res. Lett., 33, L03401, doi:10.1029/2005GL025019, 2006.
Thomas, H. and Sansom, M.: Fully coupled analysis of heat, moisture, and air transfer in unsaturated soil, J. Eng. Mech.-ASCE, 121, 392–405, 1995.
Van De Griend, A. A. and Owe, M.: Bare soil surface resistance to evaporation by vapor diffusion under semiarid conditions, Water Resour. Res., 30, 181–188, 1994.
Van Genuchten, M. T.: A closed-form equation for predicting the hydraulic conductivity of unsaturated soils, Soil Sci. Soc. Am. J., 44, 892–898, 1980.
Verma, P., Loheide, S. P., Eamus, D., and Daly, E.: Root water compensation sustains transpiration rates in an Australian woodland, Adv. Water. Resour., 74, 91–101, 2014.
Vörösmarty, C. J., Federer, C. A., and Schloss, A. L.: Potential evaporation functions compared on US watersheds: possible implications for global-scale water balance and terrestrial ecosystem modeling, J. Hydrol., 207, 147–169, 1998.
Wang, J., Cai, H., Kang, Y., and Chen, F.: Ratio of soil evaporation to the evapotranspiration for summer maize field, Nongye Gongcheng Xuebao/T. Chinese Soc. Agr. Eng., 23, 17–22, 2007.
Wang, W., Wang, Q., and Fan, J.: Relationship between air permeability, water conductivity and water content for undisturbed and disturbed soils, Nongye Gongcheng Xuebao/T. Chinese Soc. Agr. Eng., 24, 25–29, 2008.
Wei, Z., Paredes, P., Liu, Y., Chi, W. W., and Pereira, L. S.: Modelling transpiration, soil evaporation and yield prediction of soybean in North China Plain, Agr. Water Manage., 147, 43–53, 2015.
Willmott, C. J.: On the validation of models, Phys. Geogr., 2, 184–194, 1981.
Willmott, C. J., Ackleson, S. G., Davis, R. E., Feddema, J. J., Klink, K. M., Legates, D. R., O'donnell, J., and Rowe, C. M.: Statistics for the evaluation and comparison of models, J. Geophys. Res.-Oceans, 90, 8995–9005, 1985.
Wu, J., Zhang, R., and Gui, S.: Modeling soil water movement with water uptake by roots, Plant Soil, 215, 7–17, 1999.

HESSD
12, 9977–10022, 2015

Zeng, Y., Su, Z., Wan, L., Yang, Z., Zhang, T., Tian, H., Shi, X., Wang, X., and Cao, W.: Diurnal pattern of the drying front in desert and its application for determining the effective infiltration, Hydrol. Earth Syst. Sci., 13, 703–714, doi:10.5194/hess-13-703-2009, 2009a.

Zeng, Y., Wan, L., Su, Z., Saito, H., Huang, K., and Wang, X.: Diurnal soil water dynamics in the shallow vadose zone (field site of China University of Geosciences, China), Environ. Geol., 58, 11–23, 2009b.

Zeng, Y., Su, Z., Wan, L., and Wen, J.: Numerical analysis of air-water-heat flow in unsaturated soil: is it necessary to consider airflow in land surface models?, J. Geophys. Res.-Atmos., 116, D20107, doi:10.1029/2011JD015835, 2011a.

Zeng, Y., Su, Z., Wan, L., and Wen, J.: A simulation analysis of the advective effect on evaporation using a two-phase heat and mass flow model, Water Resour. Res., 47, W10529, doi:10.1029/2011WR010701, 2011b.

Zhang, B., Liu, Y., Xu, D., Cai, J., and Zhao, N.: Estimation of summer corn canopy conductance by scaling up leaf stomatal conductance, Nongye Gongcheng Xuebao/T. Chinese Soc. Agr. Eng., 27, 80–86, 2011.

Zhao, N., Liu, Y., Cai, J., Paredes, P., Rosa, R. D., and Pereira, L. S.: Dual crop coefficient modelling applied to the winter wheat–summer maize crop sequence in North China Plain: basal crop coefficients and soil evaporation component, Agr. Water Manage., 117, 93–105, 2013.

Zhou, M. C., Ishidaira, H., Hapuarachchi, H. P., Magome, J., Kiem, A. S., and Takeuchi, K.: Estimating potential evapotranspiration using Shuttleworth–Wallace model and NOAA-AVHRR NDVI data to feed a distributed hydrological model over the Mekong River basin, J. Hydrol., 327, 151–173, 2006.

Zhou, M. C., Ishidaira, H., and Takeuchi, K.: Estimation of potential evapotranspiration over the Yellow River basin: reference crop evaporation or Shuttleworth–Wallace?, Hydrol. Process., 21, 1860–1874, 2007.

HESSD
12, 9977–10022, 2015

Table 1. Crop growth stages and crop height for maize.

Crop growth stages		Date	Crop height (m)
Initial	Start	23 Jun (DOY 174)	0
Crop development	Start	6 Jul (DOY 187)	0.22
Mid-season	Start	14 Aug (DOY 226)	1.65
Late season	Start	14 Sep (DOY 257)	2.17
	Harvest	2 Oct (DOY 275)	2.17

DOY, day of the year

HESSD
12, 9977–10022, 2015

Table 2. Soil hydraulic (Van Genuchten, 1980) and thermal (De Vries, 1963) properties including saturated (θ_s) and residual (θ_r) water content; curve-fitting parameters (α and n); saturated hydraulic conductivity (K_s); specific heat capacities of the water (C_w), air (C_a), quartz (C_q), clay (C_c) and organic matter (C_o).

Soil sample	Hydraulic properties					Thermal properties				
	θ_s	θ_r	α	n	K_s	C_w	C_a	C_q	C_c	C_o
	$cm^3\,cm^{-3}$		cm^{-1}	/	$cm\,d^{-1}$	$J\,g^{-1}\,K^{-1}$				
0–20 cm	0.45	0.105	0.0045	1.41	10.50	4.18	1.01	0.80	0.90	1.92

HESSD
12, 9977–10022, 2015

Table 3. Summary statistics of correlation between observed and simulated hourly ET for each crop development stage, when using the ET_{dir} scheme and ET_{ind} scheme separately.

Crop stage	Number of observations	ET_{ind} scheme					ET_{dir} scheme				
		a	b	R^2	RMSE ($mm\,h^{-1}$)	d	a	b	R^2	RMSE ($mm\,h^{-1}$)	d
Initial	336	0.47	0.054	0.40	0.10	0.84	0.94	0.043	0.63	0.10	0.90
Crop development	936	0.69	0.064	0.70	0.10	0.94	0.81	0.041	0.78	0.09	0.96
Mid-season	744	0.62	0.055	0.80	0.11	0.93	0.89	0.027	0.90	0.08	0.98
Late season	432	0.70	0.051	0.72	0.07	0.90	0.75	0.029	0.77	0.06	0.93
Total season	2448	0.65	0.056	0.72	0.11	0.90	0.85	0.035	0.82	0.09	0.95

* The regression relation is $ET_{sim} = a \times ET_{obs} + b$; a is the slope and b is the intercept.

HESSD
12, 9977–10022, 2015

Table 4. Evaporation (E), transpiration (T), evapotranspiration (ET) and evaporation fraction (E/ET, EF) for each development stage of maize, when using the ET_{dir} scheme and ET_{ind} scheme separately. The actual evapotranspiration (ETc) was shown as well.

Crop stage	ETc (mm)	ET_{ind} scheme				ET_{dir} scheme			
		E (mm)	T (mm)	ET (mm)	EF (%)	E (mm)	T (mm)	ET (mm)	EF (%)
Initial	37.72	29.13	6.83	35.96	81.01	43.32	6.71	50.03	86.58
Crop development	140.48	34.57	122.73	157.31	21.98	45.17	107.13	152.30	29.66
Mid-season	124.74	12.15	105.75	117.91	10.31	32.01	99.26	131.26	24.38
Late season	31.23	9.50	34.22	43.72	21.73	14.10	21.66	35.77	39.43
Total season	334.18	85.36	269.53	354.89	24.05	134.60	234.76	369.37	36.44

HESSD
12, 9977–10022, 2015

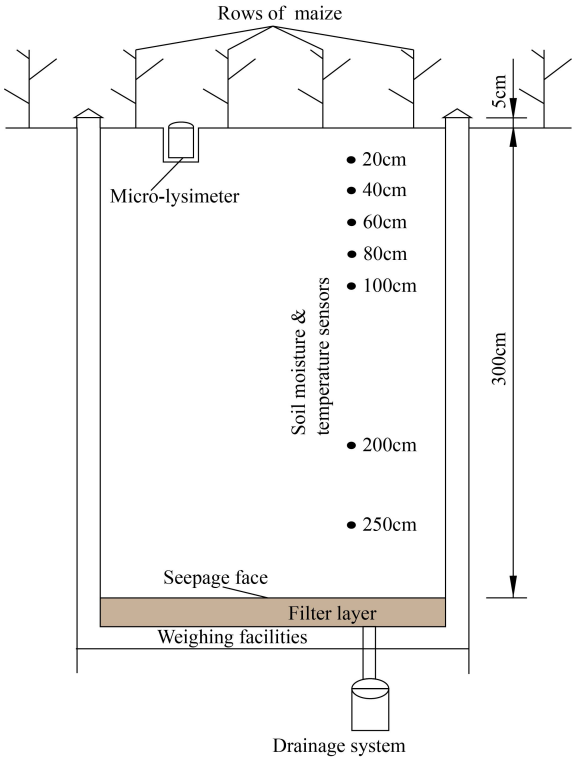

Figure 1. The schematic of the large lysimeter structure.

HESSD
12, 9977–10022, 2015

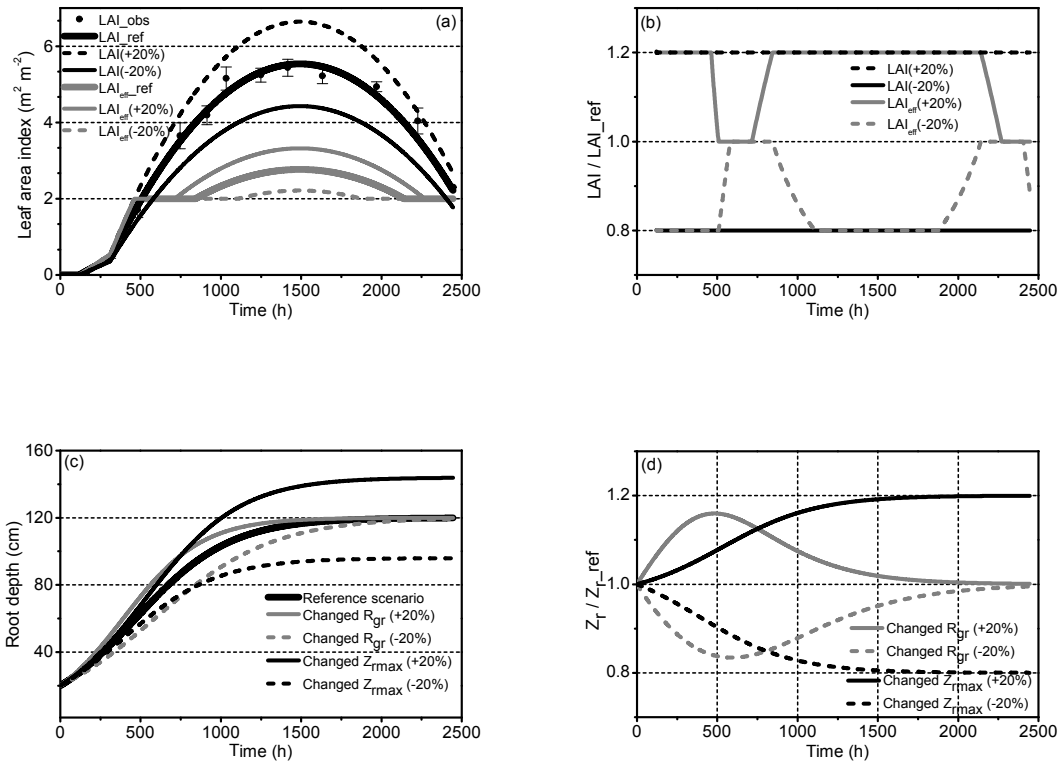

Figure 2. The seasonal variation of crop growth parameters used in the simulations: **(a)** leaf area index (LAI), **(b)** relative values of LAI compared to the reference scenario, **(c)** root depth (Z_r), and **(d)** relative values of root depth compared to the reference scenario. +20, −20 % indicate that 20 % increase or decrease based on their reference values. The vertical gridlines in **(d)** highlight the lag effect of 20 % decreased R_{gr} scenario compared to 20 % increased R_{gr} scenario.

HESSD
12, 9977–10022, 2015

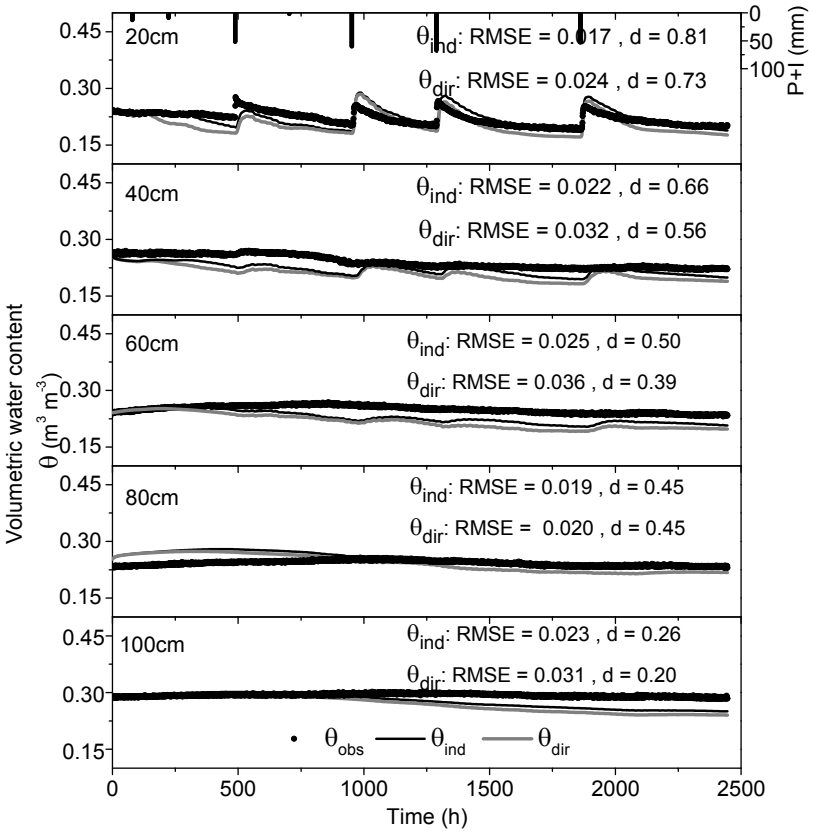

Figure 3. Comparison of observed and simulated soil volumetric water content, at selected depths: 20, 40, 60, 80 and 100 cm, with measured precipitation and irrigation (the solid black bar with the right axis of "$P + I$ (mm)"). The black dot is measurement, the solid black line is the simulation with the ET_{ind} scheme, the solid gray line is the simulation with the ET_{dir} scheme.

HESSD
12, 9977–10022, 2015

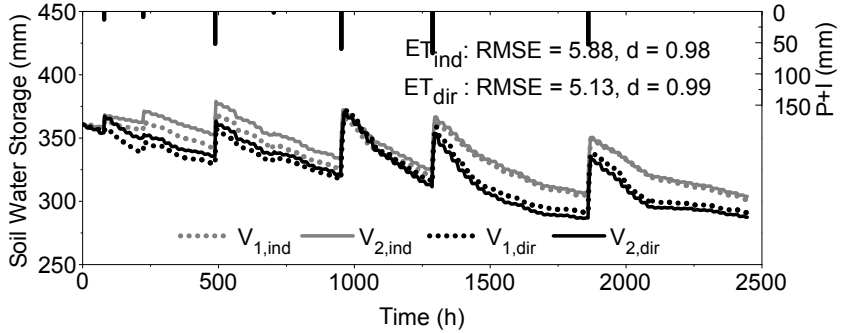

Figure 4. Comparison of simulated root-zone water storage with measured precipitation and irrigation. The gray dotted and solid lines are water storage calculated as the integration of soil water content and the inversion of water balance equation within the root-zone, using the ET_{ind} scheme, i.e. $V_{1,ind}$, $V_{2,ind}$, respectively. The black dotted and solid lines are with the ET_{dir} scheme.

HESSD
12, 9977–10022, 2015

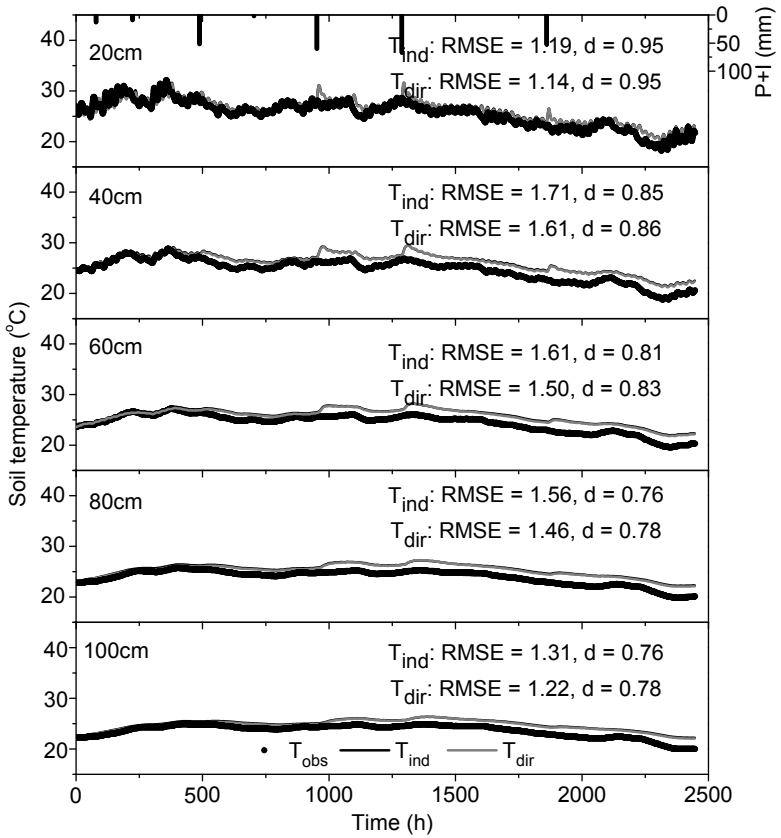

Figure 5. Comparison of observed and simulated soil temperature, at selected depths: 20, 40, 60, 80 and 100 cm, with measured precipitation and irrigation. The black dots represent the observation, the solid black line is the simulation with the ET_{ind} scheme, and the solid gray line is the simulations with the ET_{dir} scheme.

HESSD
12, 9977–10022, 2015

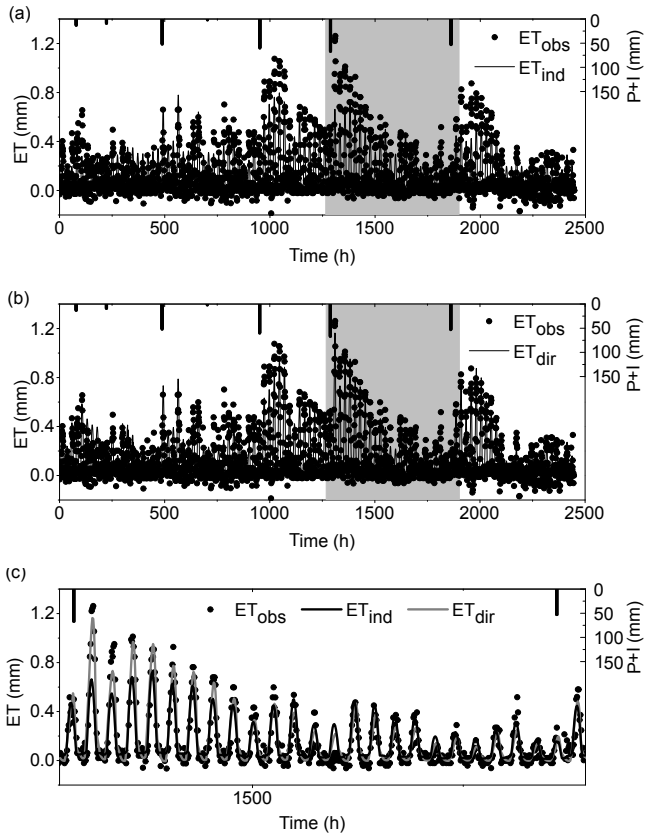

Figure 6. Diurnal variation of observed and simulated ET: **(a)** estimated using ET_{dir} scheme, **(b)** estimated using ET_{ind} scheme, **(c)** an example shows the differences between observed and simulated ET during the wet to dry cycle in the Mid-season of maize, which is highlighted by the gray shading in **(a, b)**.

HESSD
12, 9977–10022, 2015

Investigating effects of different ET schemes on soil water dynamics and ET partitioning

L. Yu et al.

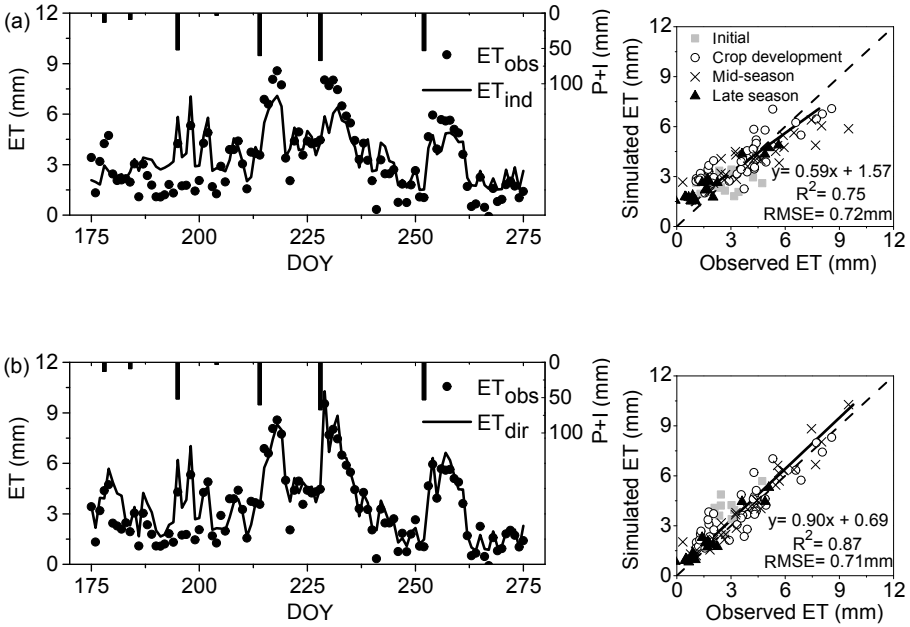

Figure 7. Daily variation of observed and simulated ET: **(a)** estimated using ET_{dir} scheme, **(b)** estimated using ET_{ind} scheme, on the right, the regression between observed and simulated ET.

HESSD
12, 9977–10022, 2015

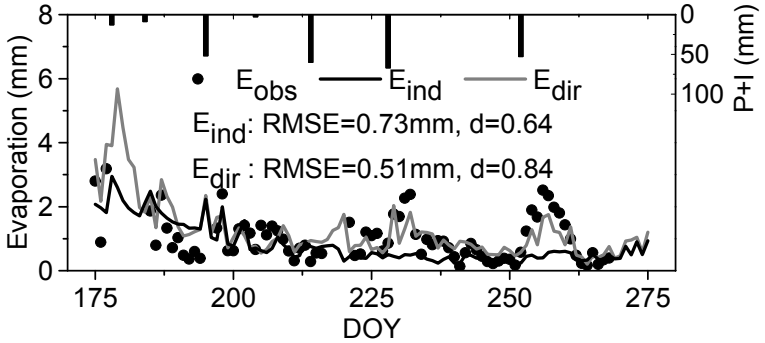

Figure 8. Daily variation of observed and simulated soil evaporation using two ET schemes.

HESSD
12, 9977–10022, 2015

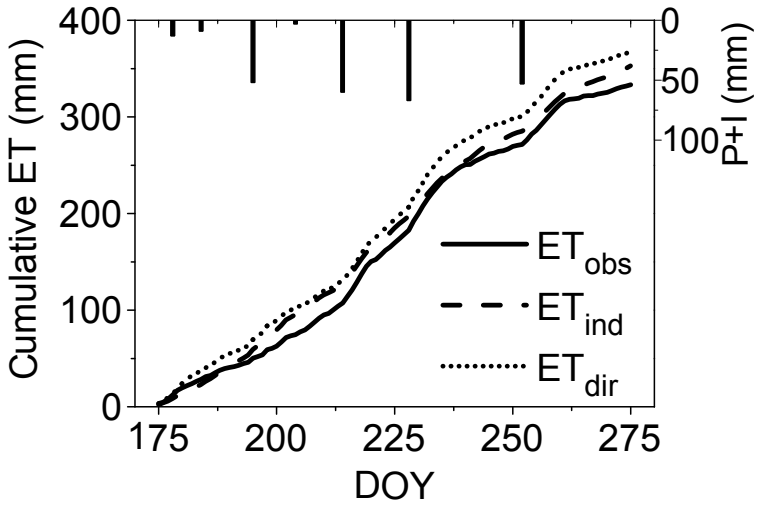

Figure 9. Cumulative variation of observed and simulated ET with the two ET schemes.

HESSD
12, 9977–10022, 2015

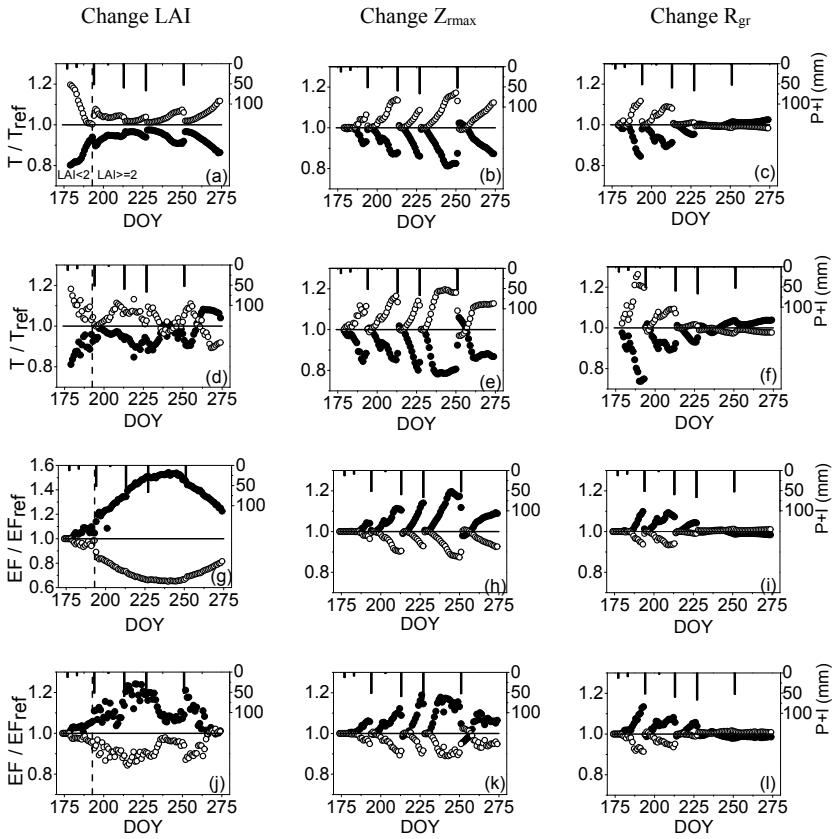

Figure 10. Relative daily variations, under changed leaf area index (LAI), maximum rooting depth (Z_{rmax}) and root growth rate (R_{gr}), of crop transpiration (**a–c**, using ET_{ind} scheme; **d–f**, using ET_{dir} scheme) and evaporation fraction (E/ET, **g–i**, using ET_{ind} scheme; **j–l**, using ET_{dir} scheme) with measured precipitation and irrigation. ∘ increase LAI, Z_{rmax} and R_{gr} by 20 %, • decrease LAI, Z_{rmax} and R_{gr} by 20 %. Note that scale for **(g)** differs from others.

HESSD
12, 9977–10022, 2015

Investigating effects of different ET schemes on soil water dynamics and ET partitioning

L. Yu et al.